A comparative study of the chemical kinetics of methyl and ethyl propanoate

A. Farooq[1,*], D. F. Davidson[2], R. K. Hanson[2], C. K. Westbrook[3]

[1]Clean Combustion Research Center, Division of Physical Sciences and Engineering, King Abdullah University of Science and Technology (KAUST), Thuwal 23955-6900, Saudi Arabia
[2]Mechanical Engineering Department, Stanford University, Stanford, CA 94305, USA
[3]Lawrence Livermore National Laboratory, CA 94550, USA

*Corresponding Author:
Aamir Farooq, PhD
Assistant Professor of Mechanical Engineering
King Abdullah University of Science & Technology (KAUST)
Building 5, Room 4217
Thuwal 23955, Kingdom of Saudi Arabia
Email: aamir.farooq@kaust.edu.sa
Tel: +966-128082704

Abstract

High temperature pyrolysis of methyl propanoate (CH_3-CH_2-C(=O)O-CH_3) and ethyl propanoate (CH_3-CH_2-C(=O)O-CH_2-CH_3) was studied behind reflected shock waves at temperatures of 1250 – 1750 K and pressure of 1.5 atm. Species time-histories were recorded for CO, CO_2, C_2H_4, and H_2O using laser absorption methods over a test time of 1 millisecond. Pyrolysis of methyl propanoate (MP) appears to be faster than that of ethyl propanoate (EP) under the present experimental conditions, where CO and CO_2 reach their plateau values faster for MP at a specific temperature and fuel concentration. Higher plateau values are reached for CO in case of MP while the CO_2 levels are similar for the two ester fuels. Ethylene production is larger for EP due to the presence of six-centered ring elimination reaction that produces ethylene and propanoic acid. Very little H_2O is produced during MP pyrolysis in contrast with appreciable H_2O production from EP. Sensitivity and rate-of-production analyses were carried out to identify key reactions that affect the measured species profiles. Previous kinetic mechanisms of Yang et al. [1, 2] and Metcalf et al. [3, 4] were used as base models and then refined to propose a new MP/EP pyrolysis mechanism.

Keywords: methyl propanoate; ethyl propanoate; biodiesel; pyrolysis; shock tube.

1. Introduction

Global warming and the world's dependence on oil as an energy source have intensified the need for more efficient energy systems and alternative sources of energy based on renewable energy technologies. The world's energy needs will increase throughout this century, driven by population and economic growth. Meeting these needs will require both the development of new energy resources, especially carbon-free ones, and the efficient and environmentally responsible utilization of fossil fuels. These trends have led to an increasing interest in the production and utilization of biofuels, like bio-alcohol and biodiesel [5-7]. Although biodiesel is gradually replacing crude-oil-derived diesel fuel, particularly in European Union, the combustion chemistry of biodiesel is not completely understood [8]. Specifically, significant work is needed on the chemical kinetics of biodiesel combustion to accurately predict the relevant emissions such as CO, particulate matter, unburnt hydrocarbons, and NOx.

Biodiesel is typically composed of a mixture of saturated and unsaturated long-chain methyl and ethyl esters. There have been only a few studies [8-12] on the chemical kinetics of these large esters because of their low vapor pressure and chemical complexity. Short chain molecules containing the same ester functional groups are thus studied to help understand the kinetic behavior of the practical fuel. A number of studies, e.g., [2, 4, 13-22], have been carried out on the oxidation and pyrolysis of methyl butanoate MB, CH_3-CH_2-CH_2-C(=O)O-CH_3, because MB contains much of the essential chemical structure of its long-chain counterparts, i.e., the methyl ester moiety and a shorter, but similar alkyl chain. There are few previous studies on the kinetics of methyl propanoate MP, CH_3-CH_2-C(=O)O-CH_3, and ethyl propanoate EP, CH_3-CH_2-C(=O)O-CH_2-CH_3. The purpose of the current study is to better understand the chemical kinetic behavior of methyl and ethyl propanoate and suggest improvements to the biodiesel chemical kinetic mechanism.

Among previous studies carried out on ethyl propanoate (EP), Blades and Gilderson [23] studied its thermal decomposition and measured the rate constant for the six-centered molecular elimination reaction producing propanoic acid $C_2H_5(C=O)OH$ and ethylene C_2H_4 over 780 – 875 K:

$$C_2H_5(C=O)OC_2H_5 \rightarrow C_2H_5(C=O)OH + C_2H_4 \quad \text{(R1)}$$

O'Neal and Benson [24] used transition state theory to calculate the activation energy of the same six-centered molecular elimination reaction of EP and found it to be in close agreement with the measured value of Blades and Gilderson [23]. Thermal decomposition of EP was also studied by Barnard et al. [25] over 913 – 1317 K using a single-pulse shock tube and their measured rate constant for the molecular elimination reaction was in good agreement with previous studies. Schwartz et al. [26] performed non-premixed flame experiments by doping methane/air with EP (and other $C_5H_{10}O_2$ isomers) and concluded that the six-centered molecular elimination reaction of EP plays a critical role in flame environments. Shock tube ignition delay times of EP and methyl butanoate were measured by Metcalfe et al. [4], who assembled a detailed chemical kinetic mechanism to show that ethyl propanoate has a faster reactivity than methyl butanoate, due largely to the fact that EP has the fast molecular elimination reaction (R1) while MB does not. Oxidation of EP in a jet-stirred reactor was used by Metcalfe et al. [3] to develop an improved chemical mechanism for ethyl propanoate. Walton et al. [22] and Yang et al. [2] made modifications to the EP mechanism of Metcalfe et al. [3, 4] to extend it to lower reaction temperatures for rapid compression machine and low-pressure laminar flame simulations. Metcalfe et al. [3] also identified the most important features of EP oxidation by carrying out a very thorough and insightful analysis of their EP oxidation mechanism. Recently, Dayma et al. [27] measured laminar burning velocities for C_4 – C_7 ethyl esters and subsequently proposed a new kinetic mechanism to describe the oxidation of the studied ethyl esters.

Hoare and Kamil [28] investigated the cool flame and ignition limits for methyl propanoate (MP) in a static reaction vessel, although no kinetic modeling was carried out. Carbon dioxide yields were measured

behind reflected shock waves by Farooq et al. [19] during thermal decomposition of MP, as well as methyl butanoate and methyl acetate, but kinetic modeling was carried out only for methyl butanoate. Yang et al. [1] developed kinetic reaction mechanisms for oxidation of MP and its corresponding unsaturated species, methyl propenoate, as well as an isomer of MP, ethyl acetate, and its unsaturated partner, vinyl acetate, to simulate low-pressure laminar flame structures for all four fuels. Very recently, Zhao et al. [29] reported species concentration measurement experiments and kinetic modeling of MP pyrolysis in a laminar flow reactor at low pressure (30 Torr) and temperatures ranging from 1000 to 1500K. The kinetic reaction mechanism proposed by Zhao et al. [29] was supplemented by original theoretical calculations of many important elementary reactions and thermochemical parameters, providing valuable new information.

Here, we present a detailed experimental study on the pyrolysis of methyl propanoate (MP) and ethyl propanoate (EP) behind reflected shock waves, using laser absorption methods to measure time-histories of four major product species: CO, CO_2, H_2O, and C_2H_4. The measurements are used to compare the reactivity of the two esters and the different decomposition pathways taken by MP and EP. Comparisons of the measured species profiles with chemical kinetic simulations are used to refine or correct the rate coefficients of key reactions. The present study has permitted us to focus on some individual reactions and reaction rates that are important in biodiesel fuel combustion but can be more directly studied in the absence of oxidizers. In particular, studying pyrolysis conditions makes it possible to use CO and CO_2 production as reaction pathway diagnostics, since in the absence of oxidizers these species are formed only from the alkyl ester moieties in MP and EP. This has practical implications because details of the production of CO and CO_2 from these structures have been identified [30] as important factors that influence the ability of alkyl ester fuels to reduce soot production in diesel engine combustion. These particular reactants, MP and EP, are structurally very similar, so the differences in their pyrolysis rates and product compositions are due entirely to the presence of either an ethyl or a methyl radical at the alkoxy site in these fuels. Since the MP/EP decomposition, H-abstraction, and

subsequent reactions producing CO, CO_2, H_2O, and C_2H_4 form a subset of the detailed biodiesel kinetic mechanism, this work will help improve the overall predictive capability of biodiesel combustion models.

2. Experimental Procedure

2.1 Shock Tube Facility

Experiments were performed in the reflected shock region of a high-purity, stainless steel, helium-driven shock tube at Stanford University. The driven section is 10.5 m long and the driver section 3.7 m long, with an inner diameter of 15.24 cm. This geometric configuration provided at least 2 ms of high-quality test time of uniform temperature and pressure for these studies. Laser absorption measurements were made at an axial location 2 cm from the end-wall. Test mixtures were prepared manometrically in a 40-liter stainless steel tank equipped with a magnetically-driven stirring vane. Between experiments, the shock tube and mixing assembly were turbo-pumped to approximately 6 μTorr. Reflected shock temperatures and pressures were determined from the incident shock speed (extrapolated to the end-wall) using standard normal shock relations, with an uncertainty of ±0.7% and ±1%, respectively. Methyl propanoate and ethyl propanoate were provided by Sigma-Aldrich at > 99% purity. Research grade (99.999%) Argon and Helium supplied by Praxair Inc. were used in the experiments.

2.2 Laser Absorption Measurements

Mid-IR quantum cascade laser absorption of CO: Carbon monoxide concentration time-histories were measured in the fundamental vibrational band of CO near 4.56 μm using a thermoelectrically-cooled quantum-cascade laser (from Alpes Lasers). The R(13) transition of the ν_1 vibrational band of CO was chosen due to its relatively high absorption strength and negligible interference from CO_2 and H_2O. The detection limit for this diagnostic is approximately 5 ppm for the conditions of these experiments. Further details about the CO

diagnostic can be found elsewhere [31]. Quantitative CO concentration (mole fraction, X_{CO}) profiles are generated from the raw traces of fractional absorption (I/I_0) using Beer-Lambert law, the measured line-strength (S), the path length L, and the measured line-shape function (ϕ):

$$I/I_0 = \exp(-S \phi P_{total} X_{CO} L) \quad (1)$$

IR diode laser absorption of CO_2: Absorption measurements of CO_2 were made using wavelength-modulation spectroscopy with second-harmonic detection (WMS-2*f*). A commercially available distributed feedback diode laser (from NanoPlus) emitting near 3633 cm^{-1} was used. This diagnostic was developed and demonstrated previously [32, 33] for the measurement of CO_2 concentration and gas temperature in shock tube kinetic experiments. Quantitative CO_2 concentration profiles were generated by comparing the measured 1*f*-normalized WMS-2*f* signals with simulated values. The WMS strategy was preferred over direct absorption to achieve higher signal-to-noise ratios in these relatively low fuel concentration experiments. This diagnostic can be used to detect minimum CO2 mole fraction of approximately 100 ppm at 1300 K and 2 atm.

IR diode laser absorption of H_2O: Water concentration time-histories were determined by measuring the absorption of 2551 nm light at the peak of an absorption feature in the ν_3 fundamental vibrational band of H_2O using a distributed feedback diode laser (from NanoPlus). A nitrogen purging system was implemented along the laser transmission path to eliminate signal loss due to absorption by ambient water vapor. The detection limit for this diagnostic is less than 50 ppm at 1200 K and 2 atm. Further details on the H_2O detection system as well as H_2O line characterization can be found elsewhere [34, 35].

CO_2 laser absorption of C_2H_4: Ethylene mole fraction was measured by taking advantage of the fortuitous overlap of the P(14) line of the CO_2 gas laser at 10.532 μm with the strong ethylene absorption band near 10.6 μm. Experiments were also conducted at an off-line wavelength of 10.675 μm to correct for interference absorption from methyl/ethyl propanoate and other hydrocarbon intermediates. The detection limit for ethylene measurements is approximately 100 ppm at 1200 K and 2 atm. Experimental details of this

165 diagnostic and high-temperature absorption cross-sections of ethylene and related alkenes are discussed by Ren
166 et al. [36] and Pilla et al. [37].

167 2.3 Modeling and Analysis

168 In recent years, significant effort has been put into steadily building a hierarchical family of chemical
169 kinetic reaction mechanisms for combustion of small alkyl ester fuels. At each step in this process, a kinetic
170 mechanism for a new alkyl ester fuel is built on an existing mechanism for smaller alkyl esters that can be
171 produced during the consumption of the larger alkyl ester molecules. Beginning with the smallest alkyl ester
172 fuels, methyl formate and ethyl formate [38], kinetic mechanisms have been extended to several other alkyl
173 ester fuels as large as methyl butanoate [2], and further studies of methyl pentanoate, methyl hexanoate, and
174 methyl 3-hexenoate are in progress. Kinetic mechanisms were produced during this process for the present
175 fuels, MP [1] and EP [2, 22], including the important kinetic modeling studies of EP combustion by Metcalfe et al.
176 [3, 4]. All of these kinetic mechanisms were validated for oxidation experiments in low-pressure premixed
177 laminar flames and ignition in a shock tube or rapid compression machine. That mechanism [1, 2], which
178 included oxidation mechanisms for both MP and EP, was then refined by upgrading its core C0 - C4 hydrocarbon
179 mechanism from Curran et al. [39]. This is the preliminary mechanism that we used to compute pyrolysis
180 histories to compare with the present experimental results.

181 Kinetic simulations of the present pyrolysis experiments, using this preliminary model, were found to be
182 sensitive to some reactions, reaction rates, and reaction pathways that had not been tested in past studies of
183 flame propagation and oxidative ignition. Some reaction rates were identified that required modification to
184 properly describe the present experimental results. The ability to use CO and CO_2 as reaction pathway
185 diagnostics, due to the unique features of fuel pyrolysis conditions, provided important evidence of the
186 shortcomings of this preliminary kinetic model. In the following sections, we illustrate some of these preliminary

187 model failures and describe the model modifications that were made, based on the simulations of the new
188 experiments and sensitivity analysis.

189 Pyrolysis is an endothermic process that leads to temperature and pressure decreases after shock
190 heating. The temperature decrease can be significant for high initial temperatures, high initial fuel
191 concentrations, relatively large fuel molecules or any combination of these factors. Since the absorption
192 coefficient is a temperature-dependent quantity, accounting for temperature change can be critical for accurate
193 species time-history determinations. When significant temperature changes occur during the measurement
194 time, it is necessary to use time-varying absorption coefficients for converting measured absorbance time-
195 histories to accurate concentration time-histories. Since temperature time-histories were not measured in this
196 study, these have been estimated from simulations using the Chemkin-Pro [40] solver with an adiabatic
197 constraint and post-reflected shock temperature and pressure calculated from normal shock relations. Shock
198 tubes are usually modeled as constant-volume (CV) although endothermicity can cause the shock tubes to
199 deviate from the ideal CV behavior and tend towards the constant-pressure (CP) mode. As demonstrated
200 previously [41, 42], although shock tubes do not exhibit pure CV or CP behavior in pyrolysis experiments,
201 predictions of temperature and species time-history are relatively insensitive to the choice between these two
202 gasdynamic models for dilute experiments. Figure 1 shows simulated temperature time-histories for 1% MP/Ar
203 and 1% EP/Ar pyrolysis. After an elapsed time of 1 ms, the CP and CV gasdynamic models predict a temperature
204 decrease of 120 $\pm$ 15 K for MP and 113 $\pm$ 13 K for EP. As expected, the temperature reduction is slightly
205 larger using CV simulation. Although neglecting such decreases in temperature can cause a significant error in
206 species time-history measurements, a $\pm$ 13 – 15 K uncertainty, resulting from using CP or CV model,
207 contributes an error of no more than $\pm$ 7% for any of the species measured here. Additionally, temperature
208 time-histories calculated using our kinetic mechanism and the Metcalfe et al. [3] mechanism are quite similar.

All experimental species profiles presented in subsequent sections are converted to mole fractions using simulated temperature profiles based on the CV model and the MP/EP kinetic mechanism of the current work.

The temperatures in Fig. 1 suggest that pyrolysis of MP is different qualitatively from pyrolysis of EP. The temperature decrease is much more abrupt for the 1% MP/99% Ar sample than for the 1% EP/99% Ar sample. The primary temperature drop takes place in a few microseconds for MP and the temperature remains nearly constant thereafter. The temperature decrease for the case of EP is much less abrupt and the temperature continues to decrease in the full 1000 μs time interval of the experimental observations.

In order to provide a framework for the discussions to follow for both the experimental and computational results, it is useful to present sample pyrolysis calculations for both fuels. The computed results, shown in Fig. 2, summarize the fuel, major intermediate species and product species mole fractions calculated using the final kinetic mechanism from the current study at a representative temperature of 1500 K. These calculations were carried out to a total elapsed time of 5 ms, long after the last experimental mole fraction measurements were made (1 ms). Similar to the temperature results shown in Fig. 1, in the case of MP pyrolysis, all of the species reach nearly constant levels in the first few microseconds, after which there are slow increases in the H_2, CO, CH_4, and C_2H_2 mole fractions and a barely perceptible decrease in the C_2H_4 level. In this sense, high-temperature pyrolysis of MP under the present conditions is comprised of a rapid first stage followed by a very long relaxation stage that leads to final chemical equilibrium. We computed this equilibrium independently for the same initial conditions (1500 K, 1.5 atm, 1% MP/Ar) and found the MP equilibrium to have a temperature of 1374 K and the only species with significant mole fractions at equilibrium were H_2 (26,710 ppm), CO (19,150 ppm), C_2H_2 (2,965 ppm), C_6H_6 (1,880 ppm), CH_4 (1,300 ppm), and C_2H_4 (130 ppm), in addition to Ar (947,780 ppm). In particular, the CO_2 mole fraction at equilibrium is about 0.001 ppm, although CO_2 is a major intermediate measured in the current experiments. Similarly, most but not all of the C_2H_4 produced in the first pyrolysis stage is ultimately consumed during the long relaxation stage. When we extended the time-dependent

pyrolysis problem of Fig. 1 and Fig. 2(a) to thousands of seconds of adiabatic elapsed time, the computed species levels and temperature eventually evolved to the corresponding values provided by the equilibrium calculation, but this relaxation time is very long compared to the 1000 μs of observation time from the current experiments.

EP pyrolysis also has a rapid first stage, followed by a much longer relaxation stage towards final equilibrium. However, in contrast with MP, EP clearly takes longer time for the first pyrolysis stage to be completed, and as we will demonstrate, its first reactive pyrolysis stage is more complex than that of MP, consisting of several distinct kinetic processes. As shown in Fig. 2(b), EP produces a greater variety of intermediate species, such as propanoic acid (C_2H_5COOH) and methyl ketene (CH_3CHCO) that are formed and then consumed with time scales longer than the initiation reactions but still much shorter than the long relaxation time to reach equilibrium. The final equilibrium conditions for EP are similar to those for MP, with H_2 (30,340 ppm), CO(19,030 ppm), C_2H_2 (2,970 ppm), C_6H_6 (3,340 ppm), CH_4 (1,900 ppm), and C_2H_4 (170 ppm) and a final equilibrium temperature of 1359 K. For EP, the most significant changes after about 5 ms are the steady but slow conversion of C_2H_4, CO_2 and H_2O to C_2H_2, H_2, and CO.

3. Results and Discussion

3.1 CO Measurements

Experimentally measured CO time-histories are shown in Fig. 3(a) and Fig. 3(b) at a variety of initial, post-shock temperatures (1259 – 1756 K) for the pyrolysis of 1% MP and 1% EP, respectively. In every experiment, for both MP and EP, CO production begins immediately at initial rates that increase with higher initial temperature. At the highest initial temperatures, CO production is immediately very fast, but that rapid production lasts for only a few microseconds, after which CO production becomes very slow. At lower temperatures, the initial rate of CO production is lower than at high temperatures but continues steadily

254 throughout the observed experimental time window of about 1 ms. As the reflected shock temperature
255 increases, the CO levels in the MP pyrolysis experiments appear to plateau to a unique value (~ 7800 ppm) at 1
256 ms. A similar trend was observed recently [20] in a study of MB pyrolysis, albeit with a higher CO plateau (~
257 10,000 ppm). For EP pyrolysis, however, the CO values at 1 ms continue to increase gradually as the initial
258 temperature increases and reach about 6200 ppm for the highest temperature studied (1756 K). Figure 3 also
259 shows that more CO is produced at 1 ms from MP compared to EP at the same initial temperature.

260 As noted above, virtually all of the oxygen in each mixture is present at equilibrium as CO, at a level of
261 about 1.9% or 19,000 ppm. Therefore, the CO levels shown in Fig. 3 for both MP and EP are snapshots in time of
262 mole fractions that would continue to increase, albeit very slowly, to final values of about 19,000 ppm. There are
263 clearly two characteristic times or stages for CO production under most of the present conditions, the first
264 shown as a rapid growth of CO to values of approximately 5,000 – 8,000 ppm, followed by a very slow second
265 stage in which the CO mole fraction increases to an equilibrium level of about 19,000 ppm. At the higher range
266 of temperatures in the current shock tube pyrolysis experiments, the first of these two time stages is very rapid
267 and is complete within the 1.0 ms observation time, but at the lower temperatures the first stage is not
268 completed before the observational time limit. Based on the experimental curves in Fig. 3, the first reaction
269 stage is completed within the available residence time for MP for temperatures above 1370 K and above 1500 K
270 for EP. The temperature decreases shown in Fig. 1 are all associated with the first of these stages, as is the
271 consumption of the fuel and any major intermediate species shown in Fig. 2.

272 A subset of experimental data from Fig. 3 are compared in Fig. 4 with kinetic simulations using the
273 preliminary kinetic mechanism [1, 2]. For MP pyrolysis, the preliminary model overestimated CO production at
274 all initial temperatures and predicted a surprisingly lower CO mole fraction at the highest initial temperature
275 (1690 K) than at lower initial temperatures of 1591 K and 1415 K. For EP pyrolysis, the preliminary model
276 underpredicted CO up to about 1560 K and overpredicted CO at higher temperatures. These computed results

277 indicated that the preliminary kinetic model couldn't reproduce the major features of the fuel pyrolysis and
278 required modifications. When the kinetic reaction mechanism was revised for both MP and EP as described in
279 the kinetic modeling section below, the computed and experimental CO mole fractions exhibited better
280 agreement, as shown in Fig. 5. We will return below to discuss further the comparisons between the
281 experimental and final kinetic modeling results.

282 Figure 6 shows CO fractional yield, defined as the ratio of CO mole fraction at 1 millisecond to the initial
283 fuel mole fraction, as a function of temperature for the two fuels. Fractional yields predicted by the preliminary
284 and revised mechanisms are also shown. As noted previously, CO yield is larger for MP compared with EP at all
285 temperatures. As the initial temperature increases, CO yield increases quite rapidly until a transition
286 temperature value is reached, above which CO yield for MP does not change noticeably and increases very
287 slowly for EP. The revised mechanism does a much better job of reproducing the measured yields compared
288 with the preliminary model.

289 ### 3.2 CO_2 Measurements

290 CO_2 experimental time-histories are shown in Fig. 7 in comparison with the revised/final kinetic
291 mechanism over a range of initial temperatures (1259 – 1599 K) and nominal pressures of 1.25 – 1.5 atm for the
292 pyrolysis of 1% methyl propanoate (MP) and 1% ethyl propanoate (EP), respectively. Experimental CO_2
293 production appears to be quite similar between the two fuels; at a specific temperature and elapsed time, the
294 CO_2 levels from the two fuels are with 20 – 30% of each other. Comparison of the measured time-histories with
295 simulations using the preliminary MP model (not shown here) indicated that the simulations overpredicted CO_2
296 at lower temperatures and underpredicted at temperatures higher than about 1400 K. For EP pyrolysis, the
297 preliminary model (not shown) underpredicted CO_2 at all temperatures by factors of 4 – 13. Significant revisions
298 to the preliminary kinetic mechanism were required to correct the CO_2 predictions. Following modifications in

299 the kinetic model, the revised model-computed CO_2 time-histories are summarized together with the
300 experimental profiles in Fig. 7. The revised kinetic mechanism will be discussed in subsequent section.

301 Figure 8 shows CO_2 fractional yield, defined as the ratio of CO_2 mole fraction at 1 millisecond to the
302 initial fuel mole fraction, as a function of temperature for the two fuels. Fractional yields predicted by the
303 preliminary as well as revised mechanism are also plotted for comparison. The experimental CO_2 yields increase
304 with increasing temperature and are quite similar for the two fuels. The preliminary kinetic mechanism
305 underpedicted CO_2 yields by a big margin for EP pyrolysis. The revised kinetic mechanism predicts much-
306 improved yields for both fuels.

307 Computed equilibrium concentrations of CO_2 are extremely small (~ 10^{-3} ppm) for both MP and EP
308 pyrolysis, so virtually all of the oxygen atoms initially present in the ester moiety are eventually found as CO at
309 equilibrium, and CO_2 production in the first stage of the present shock tube pyrolysis experiments is a temporary
310 phenomenon that completely disappears at long times in the second stage of the pyrolysis.

311 ### 3.3 Ethylene Measurements

312 Ethylene (C_2H_4) time-histories are shown in Fig. 9 over a range of initial temperatures (1354 – 1704 K)
313 and nominal pressures of 1.5 – 1.7 atm for the pyrolysis of 1% methyl propanoate (MP) and 1% ethyl
314 propanoate (EP), respectively. As expected, the presence of a second ethyl group in EP, compared with the
315 single ethyl group in MP, leads to ethylene production during EP pyrolysis that is about twice the ethylene
316 production during MP pyrolysis. Just after time zero, all of the EP decomposes to ethylene and propanoic acid.
317 Ethylene mole fractions (~ 10,000 ppm or 1%) are very close to the initial fuel mole fraction of EP, indicating that
318 nearly every EP molecule immediately produces one C_2H_4 molecule. These higher ethylene levels in EP pyrolysis
319 contribute to higher reactivity of EP compared with MP under oxidative conditions.

320 Chemical equilibrium calculations show that the eventual level of ethylene is very low (150 ppm). As
321 already noted for CO_2, the levels of ethylene shown in Fig. 9 are artifacts of the fast initial decomposition of the
322 fuel, produced in the first stage of the high-temperature pyrolysis. This ethylene is eventually consumed during
323 the slow second stage of the pyrolysis of both MP and EP fuels. Extending the pyrolysis simulations far beyond
324 the 1 ms observation time of the experiments, to 1000 seconds, confirmed that the slow relaxation reaction
325 process does indeed lead to the adiabatic distribution of species produced by the equilibrium calculation.

326 Model predictions for C_2H_4 levels, using the revised kinetic mechanism, are also shown in Fig. 9 and
327 exhibit good agreement with the experimental measurements. The kinetic model shows that the slow
328 consumption of ethylene is due to H-atom abstraction from C_2H_4 by H and OH radicals. Concentrations of these
329 radicals are higher as temperature increases, leading to a faster rate of C_2H_4 consumption as the pyrolysis
330 temperature increases, as seen in Fig. 9.

331 ### 3.4 H_2O Measurements

332 Laser absorption measurements carried out to detect H_2O during MP pyrolysis led to very weak signals
333 indicating low water production from MP. The kinetic simulations predict only about 10 – 100 ppm of H_2O within
334 the 1 ms observation time. On the other hand, large amounts of water are produced from EP and the
335 experimental results are shown in Fig. 10 over a range of temperatures (1356 – 1729 K) and nominal pressure of
336 about 1.7 atm for the pyrolysis of 1% EP/Ar. The H_2O production increases with increasing initial temperature
337 and reaches a plateau value of about 4200 ppm for temperatures higher than 1500 K. Model predictions, based
338 on the revised mechanism, are also shown in Fig. 10 and agree quite well with the experimental values. The
339 kinetic mechanism shows that water is produced from H atom abstraction reactions from ethylene and
340 propanoic acid by OH radicals under the present high-temperature pyrolysis conditions. Ethyl propanoate
341 decomposes too rapidly at these conditions to produce water from OH reactions with EP. Figure 11 shows that

342 preliminary kinetic mechanism overpredicted water fractional yield, defined as the ratio of H_2O mole fraction at
343 1 millisecond to the initial EP mole fraction, at all values of the initial temperature. The revised mechanism, on
344 the other hand, is in excellent agreement with the measured fractional yields.
345

346 # 4. Kinetic Modeling and Mechanism Improvements

347 Extensive sensitivity and reaction path analysis of MP and EP kinetic mechanisms were carried out, and a
348 number of reactions were identified that were not particularly significant under oxidation conditions but had
349 large sensitivities under pyrolysis conditions and considerable influence on computed mole fractions of the
350 species measured in the present experiments. For some of these reactions, the existing rate expressions were
351 quite uncertain. Kinetic sensitivities were calculated for both MP and EP pyrolysis at 1500K, showing the CO,
352 CO_2, C_2H_4 and H_2O sensitivities in Figures 12 – 15, respectively. Water sensitivity is only shown for EP pyrolysis as
353 very little H_2O is produced from MP, as discussed earlier. Sensitivity is defined here as the differential fractional
354 change of species mole fraction divided by the differential fractional change in the reaction rate coefficient, at a
355 given time. For each experimentally measured chemical species, there are relatively few elementary reactions to
356 which the computed species concentrations are particularly sensitive.

357 ## 4.1 Ethyl Propanoate (EP) Pyrolysis

358 Ethyl propanaote decomposes rapidly at the high temperatures of this study. As noted above, ethyl
359 esters $R_1(C=O)OC_2H_5$ react rapidly via a six-centered molecular elimination of ethylene

360 $$R_1(C=O)OC_2H_5 \rightarrow R_1(C=O)OH + C_2H_4 \qquad (R1)$$

361 while the corresponding methyl ester $R_1(C=O)OCH_3$ does not have such a fast reaction. The rate of this reaction
362 has been studied extensively and is quite well-established [23-25]. Under the present conditions, EP

363 decomposes over a period of just a few microseconds to produce propanoic acid $C_2H_5(C=O)OH$ and ethylene.
364 This is seen in Fig. 9(b) where the ethylene mole fraction in all of the 1% (i.e., 10,000 ppm) EP pyrolysis
365 experiments and model calculations rises to 10,000 ppm almost instantaneously. This can also be seen in Fig.
366 14(b) where the early-time sensitivity of reaction R1 for C_2H_4 production is very large, but the sensitivity falls to
367 zero very quickly as EP is entirely consumed. For this reason, H atom abstraction reactions with EP have
368 effectively no influence or sensitivity on the present simulations or experiments. In addition, the established
369 reaction rate expression for R1 is sufficiently accurate and has no significant sensitivity for the current results.
370 That is, large variations in the rate of reaction R1 would not change the computed results very much. The
371 present EP experiments are thus almost equivalent to experiments in which EP is replaced by equivalent
372 amounts of propanoic acid and ethylene, as discussed by Metcalfe et al. [3, 4]. At lower temperatures where the
373 rate of R1 is slower, Metcalfe et al. noted that H atom abstraction reactions can consume significant fractions of
374 EP, and this would also be true under lower temperature pyrolysis conditions, but the present experiments were
375 carried out at sufficiently high temperatures that R1 accounts for all of the EP consumption.

376 Following fast initial decomposition of EP, propanoic acid $C_2H_5(C=O)OH$ then reacts primarily via H atom
377 abstraction by H and OH with two major radical products:

378 $$C_2H_5(C=O)OH + H \rightarrow CH_3CH(C=O)OH + H_2 \quad \text{(R2)}$$

379 $$C_2H_5(C=O)OH + H \rightarrow CH_2CH_2(C=O)OH + H_2 \quad \text{(R3)}$$

380 $$C_2H_5(C=O)OH + OH \rightarrow CH_3CH(C=O)OH + H_2O \quad \text{(R4)}$$

381 $$C_2H_5(C=O)OH + OH \rightarrow CH_2CH_2(C=O)OH + H_2O \quad \text{(R5)}$$

382 Reactions R4 and R5 are major sources of water that is found as a significant product of EP
383 pyrolysis, as seen in the sensitivity analysis for H_2O in Fig. 15. The ratio of production of $CH_3CH(C=O)OH$ to that
384 of $CH_2CH_2(C=O)OH$ has a significant effect on the relative production of CO and C_2H_4 in the present experiments,

385 which can be seen in the sensitivity analyses of Figs. 12(b) and 14(b). As observed by Metcalfe et al. [3, 4],
386 $CH_3CH(C=O)OH$, produced by reactions R2 and R4, is a resonantly stabilized radical which decomposes relatively
387 slowly to produce either methyl ketene $CH_3CHC=O$ and OH or propenoic acid C_2H_3COOH and H. Methyl ketene
388 reacts quite slowly in these conditions, mostly via addition reactions of H and OH to the C=C double bond,
389 producing relatively small amounts of ethyl radicals and then ethylene, while propenoic acid decomposes to
390 produce vinyl radicals, CO and OH. Reactions R3 and R5 produce $CH_2CH_2(C=O)OH$ which then decomposes
391 rapidly via β-scission to produce ethylene and HOCO:

392 $$CH_2CH_2(C=O)OH \rightarrow C_2H_4 + HOCO \quad (R6)$$

393 This ethylene production is in addition to that formed immediately via reaction R1 and is responsible for the
394 increase of ethylene levels above 10,000 ppm in Fig. 9(b).

395 Reaction path analysis for EP pyrolysis shows that the main channel responsible for CO formation is:

396 $$HOCO \rightarrow CO + OH \quad (R7)$$

397 The same reaction path analysis also shows that the closely related reaction R8 is the main source of CO_2 in the
398 EP pyrolysis experiments:

399 $$HOCO \rightarrow CO_2 + H \quad (R8)$$

400 Thus reactions R3 and R5, followed by R6, lead to C_2H_4, CO and CO_2 production during EP pyrolysis, while
401 reactions R2 and R4 produce CO and CO_2 but do not produce ethylene. Thus ethylene production rates following
402 EP decomposition are sensitive to the ratio of (R2+R4)/(R3+R5); yet none of these reaction rates are very well
403 established. Similarly, relative production of CO and CO_2 is very sensitive to the ratios of the rates of reactions
404 R7 and R8.

405 One additional feature seen in Fig. 9(b) is that as the initial temperature increases from 1354 K to 1704
406 K, the rate of consumption of ethylene increases. Ethylene reacts primarily with H and OH to produce vinyl
407 radicals and then acetylene, and this reaction sequence accelerates as the temperature increases, resulting in
408 the more pronounced decrease in ethylene mole fractions at the highest temperatures. Reactions R7 and R8
409 produce the radical species that then react with ethylene, and reactions R7 and R8 proceed more rapidly as the
410 temperature increases. All of these processes were illustrated together in Fig. 2(b), showing initial reactant,
411 major intermediates, and the measured pyrolysis products for EP pyrolysis at an initial temperature of 1500 K.
412 The EP level falls to zero in less than 10 microseconds, producing C_2H_4 and C_2H_5COOH in equal amounts of
413 10,000 ppm. Subsequent consumption of the propanoic acid is quite rapid but is not complete by the end of the
414 experimental observation time of 1000 microseconds. Production of additional C_2H_4 as well as considerable
415 levels of H_2 and lesser amounts of H_2O, CO, C_2H_2, CO_2 and CH_3CHCO can be seen from the consumption of
416 propanoic acid. The calculations were extended to 5 ms in order to show more clearly the relative production of
417 the different species. The slow onset of net consumption of ethylene can also be seen, beginning at about 2 ms.
418 Eventually, based on further simulations carried to much longer times, as well as formal chemical equilibrium
419 calculations, the C_2H_4, CO_2, H_2O, and methyl ketene (CH_3CHCO) all are consumed.

420 A conclusion that can be drawn from the equilibrium species concentrations is that the snapshot in time
421 provided by the shock tube experiments shows, in most of the cases, a “frozen” mixture of intermediates and
422 products. Once the initial reactive stage is completed, the evolution is then very slow. As noted above, at the
423 lowest temperatures studied, the initial reactive stage is not completed before the end of the observation time
424 window, and in some cases, there is no abrupt reactive stage at all.

425 ### 4.2 Methyl Propanoate (MP) Pyrolysis

In the case of MP, unimolecular decomposition reactions of MP are quite fast at the temperatures of this study, but they do not dominate in the same manner as for EP. These reactions were written [1, 2] in the recombination direction with temperature independent rate constants, so the decomposition reaction rates were determined via detailed balance and the relevant thermochemistry of each set of reactants. Those reactions and rates were retained for the present study, and several of these reactions were found to contribute to MP decomposition at early times in the shock tube pyrolysis simulations. In declining order of their contribution to MP consumption, these are:

$$MP \rightarrow C_2H_5 + CH_3OCO \quad (R9)$$

$$MP \rightarrow CH_2COOCH_3 + CH_3 \quad (R10)$$

$$MP \rightarrow C_2H_5CO + CH_3O \quad (R11)$$

$$MP \rightarrow C_2H_5CO_2 + CH_3 \quad (R12)$$

Of these initiation reactions for MP, only reaction R12 leads to direct production of CO_2, and this reaction shows a negative sensitivity for CO production in Fig. 12(a). Two previous studies by Akih-Kumgeh and Bergthorson [43], using CBS QB3 theoretical method, and by Zhao et al. [29], using theoretical calculations at the CBS-APNO level, determined the rates of reactions R9 – R12. These reactions are written in the recombination direction in the current mechanism (see Table 1).

Since MP does not have the low activation energy molecular elimination that makes EP decomposition so fast, initiation of MP reaction is slower overall than that of EP. There is some time after the initiation where the kinetic model shows that H atom abstraction from MP is important. MP has three structurally distinct C-H bonds, and each supports H atom abstraction at a different rate. These include:

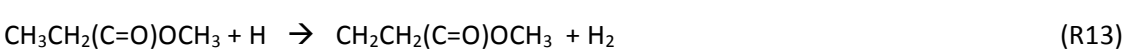

$$CH_3CH_2(C{=}O)OCH_3 + H \rightarrow CH_2CH_2(C{=}O)OCH_3 + H_2 \quad (R13)$$

447 $CH_3CH_2(C=O)OCH_3 + H \rightarrow CH_3CH(C=O)OCH_3 + H_2$ (R14)

448 $CH_3CH_2(C=O)OCH_3 + H \rightarrow CH_3CH_2(C=O)OCH_2 + H_2$ (R15)

449 as well as smaller contributions, under the present pyrolysis conditions, from H atom abstraction by OH and CH_3.

450 The radical $CH_2CH_2(C=O)OCH_3$ in reaction R13 then decomposes as:

451 $CH_2CH_2(C=O)OCH_3 \rightarrow C_2H_4 + CH_3OCO$ (R16)

452 The resonantly stable radical $CH_3CH(C=O)OCH_3$ from reaction R14 makes either methyl ketene and methoxy

453 radicals or methyl propenoate and H:

454 $CH_3CH(C=O)OCH_3 \rightarrow CH_3CH=C=O + CH_3O$ (R17)

455 or $CH_3CH(C=O)OCH_3 \rightarrow C_2H_3(C=O)OCH_3 + H$ (R18)

456 followed by $C_2H_3(C=O)OCH_3 \rightarrow C_2H_3CO + CH_3O$ (R19)

457 and the third radical $CH_3CH_2(C=O)OCH_2$ from R15 decomposes via:

458 $CH_3CH_2(C=O)OCH_2 \rightarrow C_2H_5CO + CH_2O$ (R20)

459 Rate of production (ROP) analysis for MP pyrolysis indicates that CO is produced by the following reactions:

460 $CH_3OCO \rightarrow CH_3O + CO$ (R21)

461 $C_2H_3CO \rightarrow C_2H_3 + CO$ (R22)

462 $C_2H_5CO \rightarrow C_2H_5 + CO$ (R23)

463 $HCO + M \rightarrow H + CO + M$ (R24)

464 And CO_2 is produced primarily from CH_3OCO with small contribution coming from $C_2H_5CO_2$:

465 $CH_3OCO \rightarrow CH_3 + CO_2$ (R25)

466 $C_2H_5CO_2 + M \rightarrow C_2H_5 + CO_2 + M$ (R26)

467

468 It was noted above for high-temperature EP pyrolysis that the HOCO radical provides a crucial branching
469 function by having two decomposition reactions that produce either CO or CO_2. The same function is provided
470 for MP pyrolysis by the CH_3OCO decomposition reactions R21 and R25. Decomposition reaction R9 of MP
471 produces CH_3OCO immediately. More CH_3OCO is provided from H atom abstraction reaction R13 from MP,
472 followed by the decomposition reaction R16. Reactions R21 and R25 both appear in the sensitivity plots, Fig.
473 12(a) and Fig. 13(a) for CO and CO_2, reinforcing the central role of CH_3OCO radical in MP pyrolysis.

474 Ethylene is produced from MP through R16 and the decomposition of ethyl:

475 $C_2H_5 (+M) \rightarrow C_2H_4 + H (+M)$ (R27)

476 **4.3 Mechanism Modifications**

477 Based on the sensitivities of the predicted species concentrations to the reaction pathways and rates
478 described above, modest variations were made for some of the rates to try to improve the agreement between
479 experimental and computed values. We focused our attention on a small group of reactions identified by
480 sensitivity analyses and for which rate constants were relatively uncertain.

481 For EP pyrolysis, these reactions included the two branches of the decomposition of HOCO, R7 and R8,
482 as well as the relative rates of H atom abstraction from propanoic acid (R2 – R5) that produce $CH_3CH(C=O)OH$ or
483 $CH_2CH_2(C=O)OH$, and the decomposition reactions of the resonantly stabilized $CH_3CH(C=O)OH$ radical. We
484 benefited significantly from recent studies by Barker et al. [44-47] on the kinetics of the decomposition of HOCO,
485 which above discussion noted to be particularly significant affecting the ratio of CO_2/CO produced in EP
486 pyrolysis. For the decomposition of HOCO, Metcalfe et al. [4] considered only the path producing CO and OH,

and Curran et al. [39] favored production of CO at 1500 K by a ratio of 9:1. However, both mechanisms had modeled only EP oxidation conditions, where the decomposition of HOCO has very little effect or sensitivity, in contrast with the present pyrolysis conditions. Barker et al. [47] used master equation approach with an excited HOCO* intermediate to see how the branching ratio of products (CO_2 + H or CO + OH) varies with temperature and pressure. The rates provided by Barker et al. [47] were modified slightly (~ 50%) to increase the CO_2/CO ratio. The modified rates, giving a ratio of CO_2/CO at 1500 K of about 1.9, are:

$$HOCO \rightarrow CO + OH \qquad k = 2.2 \times 10^{26}\ T^{-5.12}\ \exp(-27570/RT)\ \ cm^3mol^{-1}s^{-1}$$

$$HOCO \rightarrow CO_2 + H \qquad k = 2.0 \times 10^{36}\ T^{-8.11}\ \exp(-29060/RT)\ \ cm^3mol^{-1}s^{-1}$$

As shown in Figs. 12(b), 14(b) and 15, the relative ratio of the production of $CH_3CH(C=O)OH$ to $CH_2CH_2(C=O)OH$ has significant sensitivities on the production of CO, C_2H_4 and H_2O in the pyrolysis of EP. For these reactions, we used the rate expressions from Metcalfe et al. [3, 4] in our preliminary mechanism but increased the rate of R3, producing $CH_2CH_2(C=O)OH$, by a factor of 2 and reduced the rate of R2, which produces $CH_3CH(C=O)OH$, by a factor of 2. Thus the ratio of k2/k3 was reduced by a factor of 4 to improve the predicted levels of the measured species. Finally, rates of decomposition of the resonantly stabilized radical $CH_3CH(C=O)OH$ were modified slightly, with the rate of reaction producing methyl ketene and OH reduced by 10% and the rate of reaction producing propenoic acid and H was increased by 10%, both relative to rates taken from Metcalfe et al. [3, 4].

As discussed earlier, the decomposition of CH_3OCO plays a very critical role in controlling the CO_2/CO ratio during methyl propanoate (MP) pyrolysis. The CH_3OCO decomposition reactions R21 and R25 have been studied extensively [19, 30, 48, 49] using both theoretical and kinetic modeling approaches. In a recent shock tube and kinetic modeling study of the pyrolysis of several methyl esters, Farooq et al. [19] observed that the balance between these reactions strongly influenced the product ratio of CO_2/CO in pyrolysis of MB, and their

509 analysis suggested that the same reactions would be similarly important for pyrolysis of any methyl ester fuel.
510 The present study is very consistent with this observation. In the current work, the only significant mechanism
511 modification made to improve agreement between experimental and kinetic modeling results for MP pyrolysis
512 was to correct an error that was found in the thermochemistry of the CH_3OCO radical. It appears that the
513 number of internal rotors in the methyl formate species (the basis for the thermochemistry of its radical,
514 CH_3OCO) was inadvertently assumed to be one rotor, rather than the correct number of two, and this led to a
515 significant error in the equilibrium constant of CH_3OCO. In the current kinetic mechanism of MP/EP, the rates of
516 CH_3OCO decompositions to produce $CH_3 + CO_2$ or $CH_3O + CO$, R21 and R25, are written in the addition direction,
517 with the decomposition rates determined from the relevant equilibrium constants. The error in the number of
518 rotors produced decomposition reaction rates that favored the production of $CH_3O + CO$. When the
519 thermochemistry was corrected by Glaude [50], the two decomposition reactions of CH_3OCO strongly favored
520 production of $CH_3 + CO_2$. The sensitivity of the computed results for CO and CO_2 is evident in Figs. 12(a) and
521 13(a), and this correction in the decomposition rates made significant improvements in the computed results for
522 these species in MP pyrolysis. In particular, the corrected thermochemistry for CH_3OCO increased the rate of
523 R25 by more than a factor of 5. Our final values of the rates of reactions R21 and R25 agree well with rates used
524 in recent studies [19, 30, 48, 49]. Thermochemistry for species in kinetic reaction mechanisms can provide
525 sensitivity in computed results that can be comparable to that of reaction rate parameters, but the
526 documentation for thermochemical parameters such as bond energies, heats and entropies of formation, and
527 specific heats is not generally available. Tables of thermochemical parameters, usually provided in NASA
528 coefficient formats, are widely exchanged among kinetic modeling researchers, and it is very easy for errors like
529 that described here to occur and then be propagated rapidly amongst modeling researchers. In addition to
530 correcting the thermochemistry for CH_3OCO, the rates of the decomposition of MP were adjusted slightly to
531 decrease the CO production or increase the CO_2/CO ratio. The rates of R9 and R12 were increased by 50% and
532 the rates of R10 and R11 were reduced by 25%, all relative to rates taken from Yang et al. [1].

533 The above changes in the kinetic parameters produced the final mechanism that was used for the
534 computations summarized in Figs. 1, 2, and 5-15. The revised reaction rates used in the final mechanism are
535 summarized in Table 1. The specific reactions described in this section were found to be particularly sensitive
536 and all of them had not been tested or refined by previous kinetic modeling studies that were based on
537 oxidation experiments. Use of pyrolysis conditions made it possible to have sufficient sensitivity to them to
538 suggest corrections in their reaction rates. Improved rates have been determined for them, but the real result of
539 the present kinetic modeling is that further studies of these reactions would be desirable. Four of these
540 reactions involve complex decompositions of CH_3OCO and HOCO, which proceed via excited intermediate
541 adducts, and others involve branching ratios of hydrocarbon radicals, some involving resonantly stabilized
542 reactants or products.

543 Recently, there has been an increased interest in the chemical kinetics community to carry out
544 uncertainty analysis of reaction mechanisms and the use of global uncertainty analysis tools for theoretical
545 kinetics studies [51-53]. Such involved methods are beyond the scope of current work. However, a simple
546 estimation-based analysis was carried out to estimate the uncertainty in the proposed Arrhenius pre-
547 exponential factors. If f_k is the uncertainty factor of the rate coefficient, the uncertainty limits of the rate
548 parameters are $A_k f_k$ and A_k/f_k. The uncertainty factors are given in Table 1 for the reactions modified in the
549 current work. These uncertainty factors are obtained by considering the measurement uncertainty and the
550 sensitivity of the measured species to these rate constants. As discussed earlier, the combination of rate
551 constants proposed here provide improved predictions of the species measured during MP and EP pyrolysis. For
552 the uncertainty analysis, one specific rate constant was varied till it provided improved prediction of the species
553 most sensitive to that rate constant. Measured profiles of CO and CO_2 are very sensitive to HOCO and CH_3OCO
554 decomposition and this leads to relatively small uncertainty factors for reactions R7, R8, R21 and R25. Other rate
555 constants are assigned relatively large uncertainty factors due to complicated sensitivities of measured species

to these reactions. However, for all reactions listed in Table 1, the assigned uncertainty factors are smaller than those in the original mechanisms.

5. Conclusions

Concentration time-histories of CO, CO_2, C_2H_4, and H_2O were measured using shock tube / laser absorption methods to study the high temperature pyrolysis of methyl propanaote (MP) and ethyl propanoate (EP). The measured species time-histories are used to elaborate the effect of structural difference (methyl vs ethyl) on the production of radical, intermediate, and product species. Both fuels exhibit a two-stage pyrolysis process – a rapid first stage followed by a long relaxation stage leading to equilibrium. The present experimental conditions and available test times target the first pyrolysis stage where MP decays faster than EP. The pyrolysis of EP is initiated entirely by the six-centered molecular elimination reaction (R1) that makes ethylene and propanoic acid. This is followed by H abstraction reactions of propanoic acid and eventually the formation of HOCO radical which determines the ratio of CO/CO_2 production. Updating the rate constants of HOCO decomposition pathways and H abstractions of propanoic acid led to much-improved agreement between the experimental species data and model predictions. The pyrolysis of MP, on the other hand, is controlled initially by unimolecular decomposition and H abstraction reactions of MP. These reactions produce the important CH_3OCO radical which controls CO/CO_2 production much like the HOCO radical in EP pyrolysis. The updated rate constant / thermochemistry for the decomposition of CH_3OCO resulted in excellent agreement between measured and simulated concentrations. We believe that the refined pyrolysis mechanism for MP/EP will be very useful for the development of a comprehensive and validated chemical kinetic mechanism for biodiesel combustion.

Acknowledgments

The work of Prof. Farooq was supported by the Clean Combustion Research Center at King Abdullah University of Science and Technology (KAUST). The experiments were performed at Stanford University. The work of the Stanford University authors was supported as part of the CEFRC, an Energy Frontier Research Center funded by the U.S. Department of Energy, Office of Science, Basic Energy Sciences under Award # DE-SC0001198. The work by Dr. Westbrook was supported by the US Department of Energy, Office of Vehicle Technologies and the Office of Basic Energy Sciences and was performed under the auspices of the US Department of Energy by Lawrence Livermore National Laboratory under Contract DE-AC52-07NA27344.

Supplementary Material

The kinetic and thermodynamic files for the final mechanism are provided as supplementary material.

References

[1] Yang B, Westbrook CK, Cool TA, Hansen N, Kohse-Höinghaus K. The effect of carbon-carbon double bonds on the combustion chemistry of small fatty acid esters. Z Phys Chem. 2011;225:1293-314.

[2] Yang B, Westbrook CK, Cool TA, Hansen N, Kohse-Höinghaus K. Fuel-specific influences on the composition of reaction intermediates in premixed flames of three C5H10O2 ester isomers. PCCP. 2011;13:6901-13.

[3] Metcalfe W, Togbé C, Dagaut P, Curran H, Simmie J. A jet-stirred reactor and kinetic modeling study of ethyl propanoate oxidation. Combust Flame. 2009;156:250-60.

[4] Metcalfe W, Dooley S, Curran H, Simmie J, El-Nahas A, Navarro M. Experimental and modeling study of C5H10O2 ethyl and methyl esters. The Journal of Physical Chemistry A. 2007;111:4001-14.

[5] Kahraman B. Biodiesel as an alternative motor fuel: Production and policies in the European Union. Renewable and Sustainable Energy Reviews. 2008;12:542-52.

[6] Ayhan D. Potential applications of renewable energy sources, biomass combustion problems in boiler power systems and combustion related environmental issues. Prog Energy Combust Sci. 2005;31:171-92.

[7] Kohse-Höinghaus K, Oßwald P, Cool TA, Kasper T, Hansen N, Qi F, et al. Biofuel combustion chemistry: from ethanol to biodiesel. Angew Chem Int Ed. 2010;49:3572-97.

[8] Westbrook CK, Naik CV, Herbinet O, Pitz WJ, Mehl M, Sarathy SM, et al. Detailed chemical kinetic reaction mechanisms for soy and rapeseed biodiesel fuels. Combust Flame. 2011;158:742-55.

[9] Herbinet O, Pitz WJ, Westbrook CK. Detailed chemical kinetic oxidation mechanism for a biodiesel surrogate. Combust Flame. 2008;154:507-28.

[10] Dagaut P, Gaı¨l S, Sahasrabudhe M. Rapeseed oil methyl ester oxidation over extended ranges of pressure, temperature, and equivalence ratio: Experimental and modeling kinetic study. Proc Combust Inst. 2007;31:2955-61.

[11] Zhang Y, Yang Y, Boehman AL. Premixed ignition behavior of C9 fatty acid esters: A motored engine study. Combust Flame. 2009;156:1202-13.

[12] Herbinet O, Pitz WJ, Westbrook CK. Detailed chemical kinetic mechanism for the oxidation of biodiesel fuels blend surrogate. Combust Flame. 2010;157:893-908.

[13] Dooley S, Curran HJ, Simmie JM. Autoignition measurements and a validated kinetic model for the biodiesel surrogate, methyl butanoate. Combust Flame. 2008;153:2-32.

[14] Lin KC, Lai JYW, Violi A. The role of the methyl ester moiety in biodiesel combustion: A kinetic modeling comparison of methyl butanoate and n-butane. Fuel. 2012;92:16-26.

[15] Walton SM, Karwat DM, Teini PD, Gorny AM, Wooldridge MS. Speciation studies of methyl butanoate ignition. Fuel. 2011;90:1796-804.

[16] Szybist JP, McFarlane J, Bunting BG. Comparison of Simulated and Experimental Combustion of Biodiesel Blends in a Single Cylinder Diesel HCCI Engine. Journal Name: Journal of the Society of Automotive Engineers of Japan. 2007:Medium: X; Size: 1.

[17] Huynh LK, Violi A. Thermal Decomposition of Methyl Butanoate: Ab Initio Study of a Biodiesel Fuel Surrogate. The Journal of Organic Chemistry. 2007;73:94-101.

[18] Gaïl S, Thomson MJ, Sarathy SM, Syed SA, Dagaut P, Diévart P, et al. A wide-ranging kinetic modeling study of methyl butanoate combustion. Proc Combust Inst. 2007;31:305-11.

[19] Farooq A, Davidson DF, Hanson RK, Huynh LK, Violi A. An experimental and computational study of methyl ester decomposition pathways using shock tubes. Proc Combust Inst. 2009;32:247-53.

[20] Farooq A, Ren W, Lam KY, Davidson DF, Hanson RK, Westbrook CK. Shock tube studies of methyl butanoate pyrolysis with relevance to biodiesel. Combust Flame. 2012.

[21] Fisher EM, Pitz WJ, Curran HJ, Westbrook CK. Detailed chemical kinetic mechanisms for combustion of oxygenated fuels. Proc Combust Inst. 2000;28:1579-86.
[22] Walton S, Wooldridge M, Westbrook C. An experimental investigation of structural effects on the auto-ignition properties of two C< sub> 5</sub> esters. Proc Combust Inst. 2009;32:255-62.
[23] Blades AT, Gilderson P. Kinetics of the thermal decomposition of ethyl propionate. Can J Chem. 1960;38:1412-5.
[24] O'Neal H, Benson S. A Method for Estimating the Arrhenius A Factors for Four-and Six-Center Unimolecular Reactions. The Journal of Physical Chemistry. 1967;71:2903-21.
[25] Barnard JA, Cocks AT, Parrott TK. Thermal unimolecular decomposition of ethyl propionate behind reflected shock waves. Journal of the Chemical Society, Faraday Transactions 1: Physical Chemistry in Condensed Phases. 1976;72:1456-63.
[26] Schwartz WR, McEnally CS, Pfefferle LD. Decomposition and hydrocarbon growth processes for esters in non-premixed flames. The Journal of Physical Chemistry A. 2006;110:6643-8.
[27] Dayma G, Halter F, Foucher F, Mounaim-Rousselle C, Dagaut P. Laminar Burning Velocities of C4–C7 Ethyl Esters in a Spherical Combustion Chamber: Experimental and Detailed Kinetic Modeling. Energy & Fuels. 2012;26:6669-77.
[28] Hoare D, Kamil M. The combustion of ethyl acetate, methyl propionate, and< i> i</i>-propyl acetate. Combust Flame. 1970;15:61-70.
[29] Zhao L, Xie M, Ye L, Cheng Z, Cai J, Li Y, et al. An experimental and modeling study of methyl propanoate pyrolysis at low pressure. Combust Flame. 2013.
[30] Westbrook CK, Pitz WJ, Curran HJ. Chemical Kinetic Modeling Study of the Effects of Oxygenated Hydrocarbons on Soot Emissions from Diesel Enginesâ€ The Journal of Physical Chemistry A. 2006;110:6912-22.
[31] Ren W, Farooq A, Davidson D, Hanson R. CO concentration and temperature sensor for combustion gases using quantum-cascade laser absorption near 4.7 µm. Appl Phys B. 2012;107:849-60.
[32] Farooq A, Jeffries JB, Hanson RK. Measurements of CO2 concentration and temperature at high pressures using 1f-normalized wavelength modulation spectroscopy with second harmonic detection near 2.7 µm. Appl Opt. 2009;48:6740-53.
[33] Farooq A, Jeffries JB, Hanson RK. Sensitive detection of temperature behind reflected shock waves using wavelength modulation spectroscopy of CO2 near 2.7 µm. Applied Physics B: Lasers and Optics. 2009;96:161-73.
[34] Hong Z, Farooq A, Barbour EA, Davidson DF, Hanson RK. Hydrogen Peroxide Decomposition Rate: A Shock Tube Study Using Tunable Laser Absorption of H2O near 2.5 µm. The Journal of Physical Chemistry A. 2009;113:12919-25.
[35] Farooq A, Jeffries JB, Hanson RK. In situ combustion measurements of H2O and temperature near 2.5 µm using tunable diode laser absorption. Meas Sci Technol. 2008;19:075604.
[36] Ren W, Davidson DF, Hanson RK. IR laser absorption diagnostic for C2H4 in shock tube kinetics studies. Int J Chem Kinet. 2012;44:423-32.
[37] Pilla GL, Davidson DF, Hanson RK. Shock tube/laser absorption measurements of ethylene time-histories during ethylene and n-heptane pyrolysis. Proc Combust Inst. 2011;33:333-40.
[38] Westbrook CK, Pitz WJ, Westmoreland PR, Dryer FL, Chaos M, Oßwald P, et al. A detailed chemical kinetic reaction mechanism for oxidation of four small alkyl esters in laminar premixed flames. Proc Combust Inst. 2009;32:221-8.
[39] Metcalfe WK, Burke SM, Ahmed SS, Curran HJ. A Hierarchical and Comparative Kinetic Modeling Study of C1− C2 Hydrocarbon and Oxygenated Fuels. Int J Chem Kinet. 2013;45:638-75.
[40] CHEMKIN-PRO-15112. Reaction Design. 2012;San Diego.
[41] Stranic I, Pyun SH, Davidson DF, Hanson RK. Multi-species measurements in 1-butanol pyrolysis behind reflected shock waves. Combust Flame. 2012.

[42] Pyun SH, Ren W, Davidson DF, Hanson RK. Methane and ethylene time-history measurements in< i> n</i>-butane and< i> n</i>-heptane pyrolysis behind reflected shock waves. Fuel. 2012.
[43] Akih-Kumgeh B, Bergthorson JM. Structure-reactivity trends of C1–C4 alkanoic acid methyl esters. Combust Flame. 2011;158:1037-48.
[44] Weston Jr RE, Nguyen TL, Stanton JF, Barker JR. HO+ CO Reaction Rates and H/D Kinetic Isotope Effects: Master Equation Models with ab Initio SCTST Rate Constants. The Journal of Physical Chemistry A. 2013;117:821-35.
[45] Barker JR. Energy transfer in master equation simulations: A new approach. Int J Chem Kinet. 2009;41:748-63.
[46] Nguyen TL, Xue BC, Weston Jr RE, Barker JR, Stanton JF. Reaction of HO with CO: Tunneling Is Indeed Important. The Journal of Physical Chemistry Letters. 2012;3:1549-53.
[47] Barker JR. Personal communication. 2013.
[48] Glaude PA, Pitz WJ, Thomson MJ. Chemical kinetic modeling of dimethyl carbonate in an opposed-flow diffusion flame. Proc Combust Inst. 2005;30:1111-8.
[49] McCunn LR, Lau K-C, Krisch MJ, Butler LJ, Tsung J-W, Lin JJ. Unimolecular dissociation of the CH3OCO radical: an intermediate in the CH3O+ CO reaction. The Journal of Physical Chemistry A. 2006;110:1625-34.
[50] Glaude P-A. Personal communication. 2013.
[51] Klippenstein SJ, Harding LB, Davis MJ, Tomlin AS, Skodje RT. Uncertainty driven theoretical kinetics studies for CH3OH ignition: HO2 + CH3OH and O2 + CH3OH. Proc Combust Inst. 2011;33:351-7.
[52] Tomlin A, Ziehn T. The Use of Global Sensitivity Methods for the Analysis, Evaluation and Improvement of Complex Modelling Systems. In: Gorban AN, Roose D, editors. Coping with Complexity: Model Reduction and Data Analysis: Springer Berlin Heidelberg; 2011. p. 9-36.
[53] Davis MJ, Skodje RT, Tomlin AS. Global Sensitivity Analysis of Chemical-Kinetic Reaction Mechanisms: Construction and Deconstruction of the Probability Density Function. The Journal of Physical Chemistry A. 2011;115:1556-78.

Tables

Table 1: Rate constants used in the final MP/EP pyrolysis mechanism.

	Reaction	A	n	E	f_k
R2	$C_2H_5(C=O)OH + H \rightarrow CH_3CH(C=O)OH + H_2$	6.25E+13	0	7300	1.6
R3	$C_2H_5(C=O)OH + H \rightarrow CH_2CH_2(C=O)OH + H_2$	2.60E+06	2.54	6756	1.6
R7	$HOCO \rightarrow CO + OH$	2.20E+26	-5.12	27570	1.25
R8	$HOCO \rightarrow CO_2 + H$	2.00E+36	-8.11	29060	1.25
R9	$C_2H_5 + CH_3OCO \rightarrow MP$	1.20E+13	0	0	1.4
R10	$CH_2COOCH_3 + CH_3 \rightarrow MP$	7.50E+12	0	0	1.7
R11	$C_2H_5CO + CH_3O \rightarrow MP$	6.00E+13	0	0	1.7
R12	$C_2H_5CO_2 + CH_3 \rightarrow MP$	1.50E+13	0	0	1.4
R21	$CH_3O + CO \rightarrow CH_3OCO$	1.55E+06	2.02	5730	1.20
R25	$CH_3 + CO_2 \rightarrow CH_3OCO$	4.76E+07	1.54	34700	1.20

Notes:

(a) $k = AT^n\exp(-E/RT)$, The units are in cm^3, mol, s, cal.

(b) MP = $CH_3CH_2(C=O)CH_3$

(c) f_k is the uncertainty factor

(d) These rate constants are optimized over the measured temperature range (1250 – 1750 K)

716 **Figures**

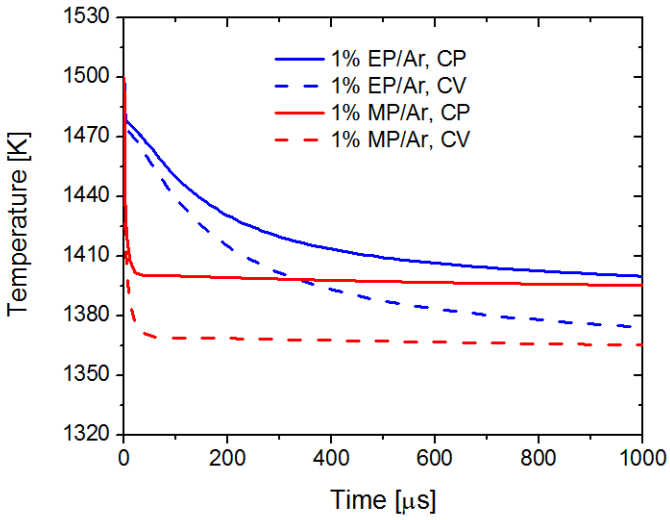

717

718 Figure 1. Simulated temperature using the present kinetic mechanism with constant pressure (CP) and

719 constant volume (CV) adiabatic constraints. Initial conditions: T = 1500 K, P = 1.5 atm.

720

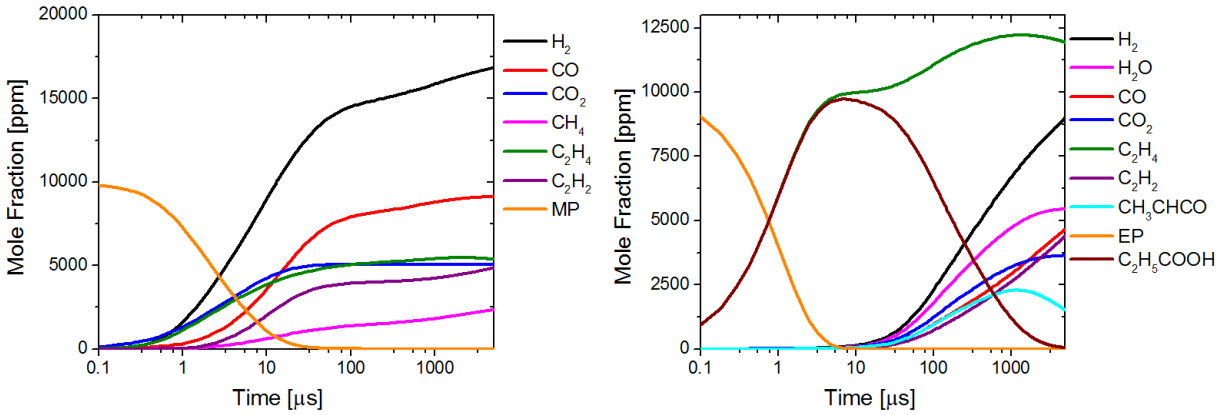

(a) (b)

Figure 2. Computed species mole fractions using the final MP/EP kinetic mechanism from current work for (a) 1% MP/Ar, (b) 1% EP/Ar. Initial conditions: T = 1500 K, P = 1.5 atm.

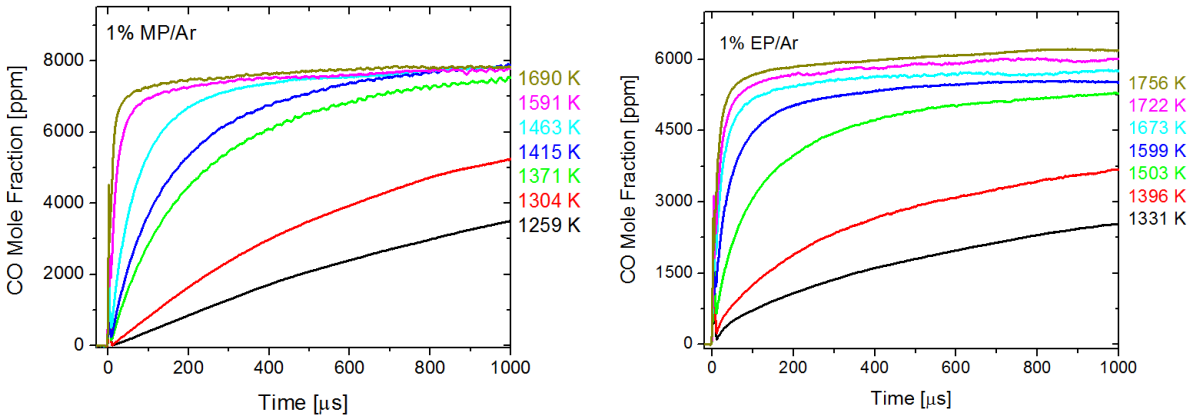

(a) (b)

Figure 3. Measured CO mole fraction profiles during the pyrolysis of (a) 1% MP/Ar, (b) 1% EP/Ar. Reflected shock temperatures are shown, whereas reflected shock pressures range from 1.25 to 1.5 atm.

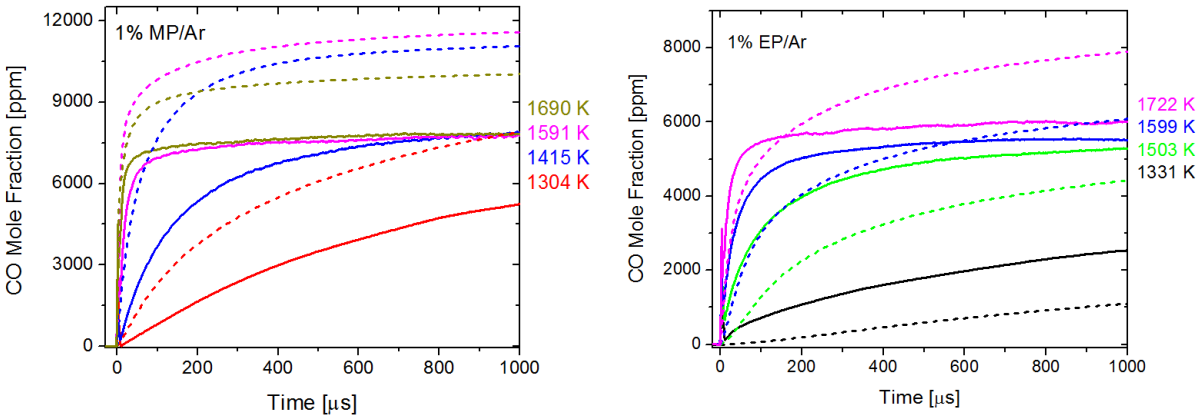

(a) (b)

Figure 4. Comparison of measured CO profiles (solid lines) with simulations (dash lines) using the preliminary kinetic mechanism [1, 2]. Reflected shock temperatures are shown, whereas reflected shock pressures range from 1.25 to 1.5 atm.

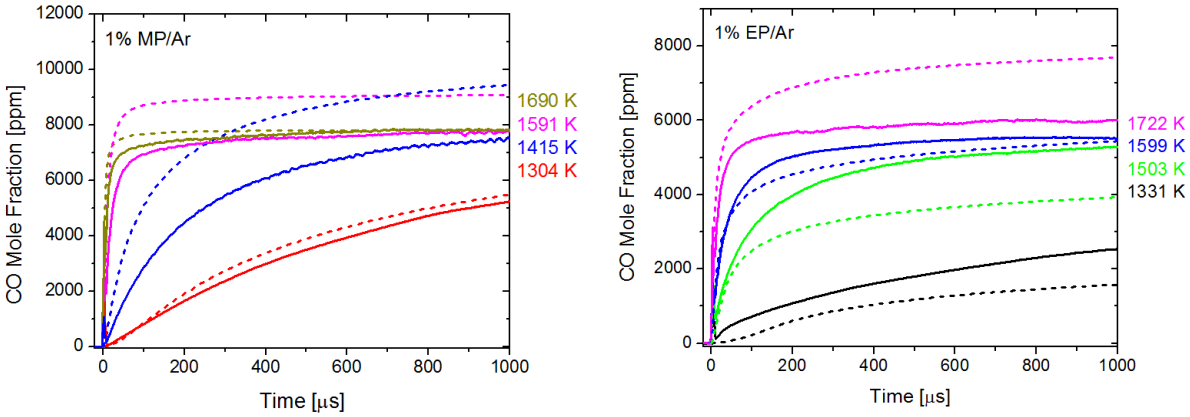

(a) (b)

Figure 5. Comparison of measured CO profiles (solid lines) with simulations (dash lines) using the final MP/EP kinetic mechanism from current work. Experimental conditions are same as in Fig. 4.

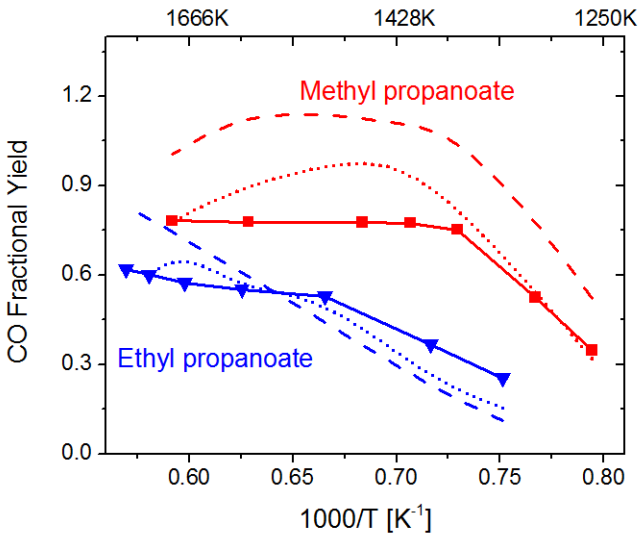

Figure 6. CO fractional yield (ratio of CO mole fraction at 1 ms to the initial fuel mole fraction) for 1% MP/Ar and 1% EP/Ar pyrolysis. Symbols (connected by solid lines) represent measurements, dashed lines are predictions using the preliminary mechanism, and dotted lines are predictions using the final mechanism.

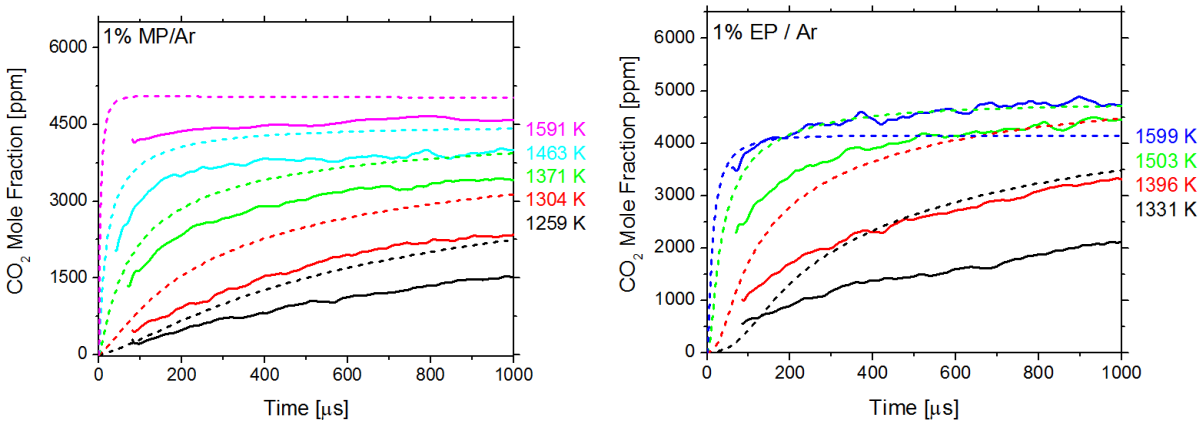

(a) (b)

Figure 7. Comparison of measured CO profiles (solid lines) with simulations (dash lines) using the final MP/EP kinetic mechanism from current work. Reflected shock temperatures are shown, whereas reflected shock pressures range from 1.25 to 1.5 atm.

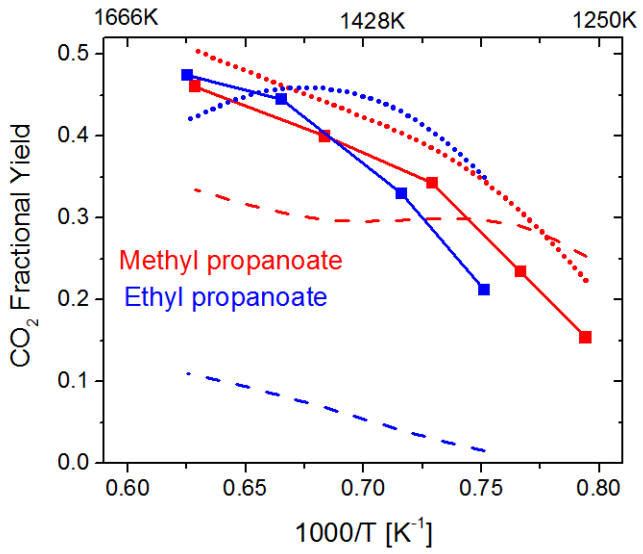

777

778 Figure 8. CO_2 fractional yield (ratio of CO_2 mole fraction at 1 ms to the initial fuel mole fraction) for 1%

779 MP/Ar and 1% EP/Ar pyrolysis. Symbols (connected by solid lines) represent measurements, dashed

780 lines are predictions using the preliminary mechanism, and dotted lines are predictions using the final

781 mechanism.

782

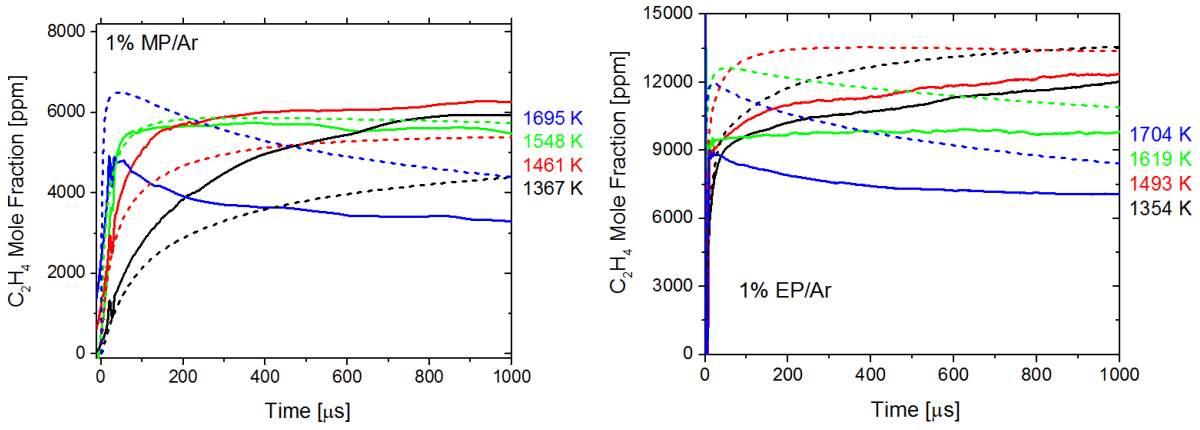

(a) (b)

Figure 9. Comparison of measured ethylene profiles (solid lines) with simulations (dash lines) using the final MP/EP kinetic mechanism from current work. Reflected shock temperatures are shown, whereas reflected shock pressures range from 1.5 to 1.7 atm.

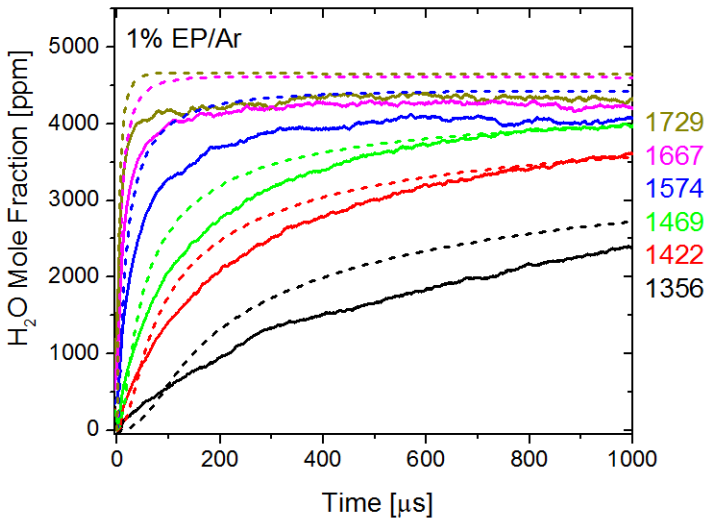

Figure 10. Comparison of measured water profiles (solid lines) with simulations (dash lines) using the final MP/EP kinetic mechanism from current work. Reflected shock temperatures are shown, whereas reflected shock pressures range from 1.5 to 1.7 atm.

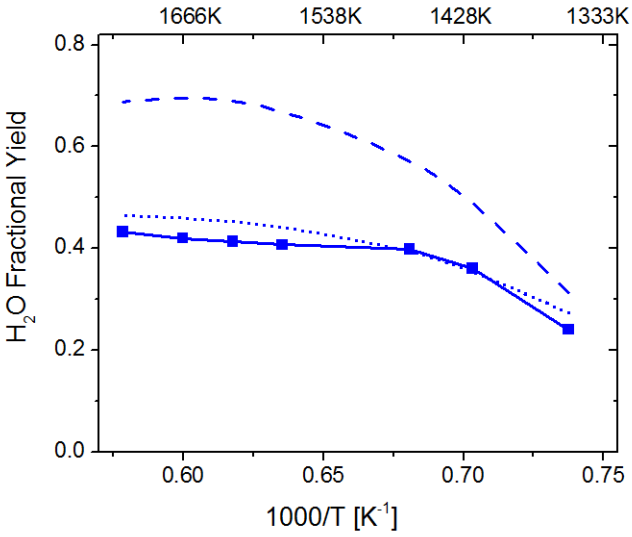

796

797 Figure 11. Water fractional yield (ratio of H_2O mole fraction at 1 ms to the initial fuel mole fraction) for
798 1% EP/Ar pyrolysis. Symbols (connected by solid lines) represent measurements, dashed line is the
799 prediction using the preliminary mechanism, and dotted line is the prediction using the final mechanism.

800

801

802

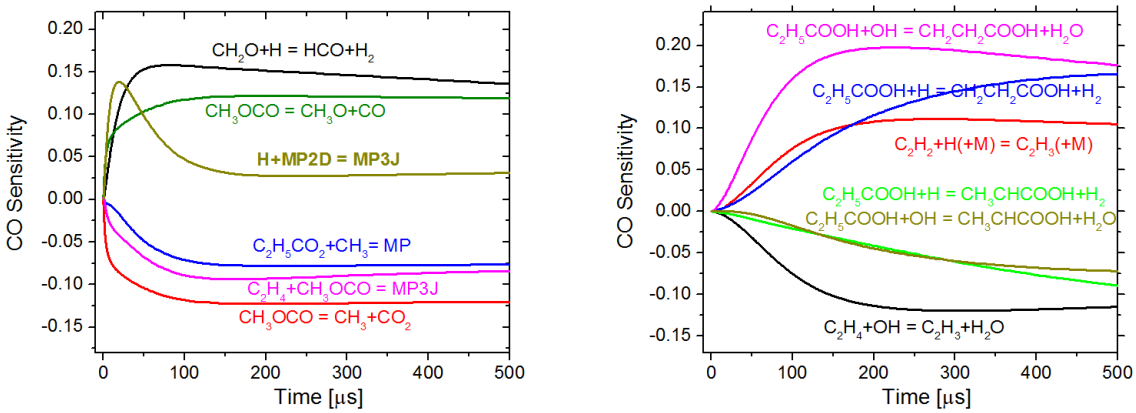

(a) (b)

Figure 12. CO sensitivity for (a) 1% MP/Ar, (b) 1% EP/Ar pyrolysis. Initial conditions: T = 1500 K, P = 1.5 atm.

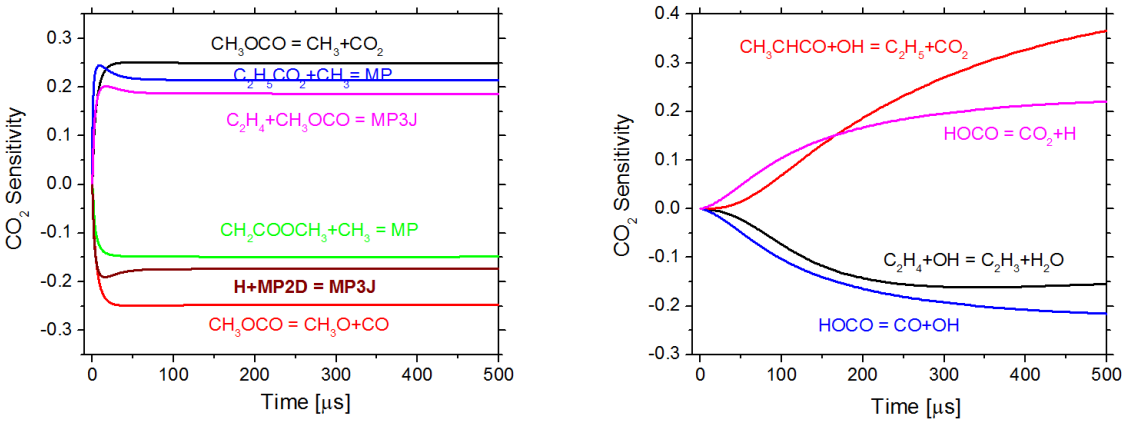

(a) (b)

Figure 13. CO_2 sensitivity for (a) 1% MP/Ar, (b) 1% EP/Ar pyrolysis. Initial conditions: T = 1500 K, P = 1.5 atm.

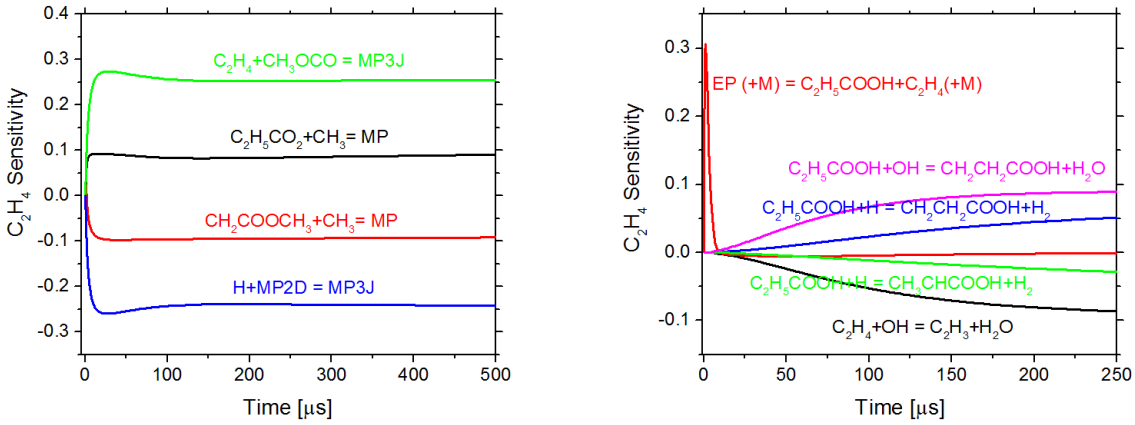

(a) (b)

Figure 14. Ethylene sensitivity for (a) 1% MP/Ar, (b) 1% EP/Ar pyrolysis. Initial conditions: T = 1500 K, P = 1.5 atm.

822

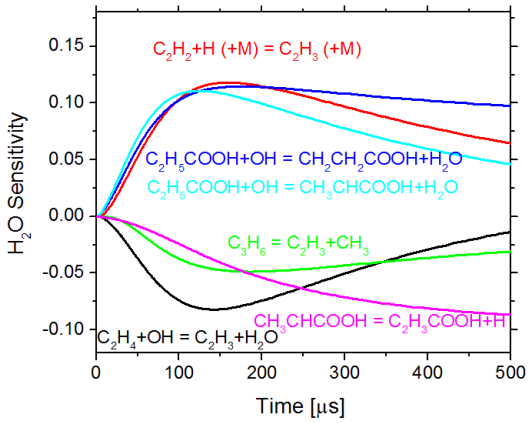

823

824 Figure 15. H_2O sensitivity for 1% EP/Ar pyrolysis. Initial conditions: T = 1500 K, P = 1.5 atm.

825